

Constraints on the superconducting order parameter in Sr₂RuO₄ from oxygen-17 nuclear magnetic resonance

A. Pustogow^{1,8}*, Yongkang Luo^{1,2,8}*, A. Chronister¹, Y.–S. Su¹, D. A. Sokolov³, F. Jerzembeck³, A. P. Mackenzie^{3,4}, C. W. Hicks³, N. Kikugawa⁵, S. Raghu⁶, E. D. Bauer⁷ & S. E. Brown¹*

Phases of matter are usually identified through spontaneous symmetry breaking, especially regarding unconventional superconductivity and the interactions from which it originates. In that context, the superconducting state of the quasi-two-dimensional and strongly correlated perovskite Sr₂RuO₄ is considered to be the only solid-state analogue to the superfluid ³He-A phase ^{1,2}, with an odd-parity order parameter that is unidirectional in spin space for all electron momenta and breaks time-reversal symmetry. This characterization was recently called into question by a search for an expected 'split' transition in a Sr₂RuO₄ crystal under in-plane uniaxial pressure, which failed to find any such evidence; instead, a dramatic rise and a peak in a single-transition temperature were observed^{3,4}. Here we use nuclear magnetic resonance (NMR) spectroscopy of oxygen-17, which is directly sensitive to the order parameter via hyperfine coupling to the electronic spin degrees of freedom, to probe the nature of superconductivity in Sr₂RuO₄ and its evolution under strain. A reduction of the Knight shift is observed for all strain values and at temperatures below the critical temperature, consistent with a drop in spin polarization in the superconducting state. In unstrained samples, our results contradict a body of previous NMR work reporting no change in the Knight shift⁵ and the most prevalent theoretical interpretation of the order parameter as a chiral p-wave state. Sr₂RuO₄ is an extremely clean layered perovskite and its superconductivity emerges from a strongly correlated Fermi liquid, and our work imposes tight constraints on the order parameter symmetry of this archetypal system.

The normal state of Sr_2RuO_4 has three bands crossing the Fermi level^{6,7}, with pronounced strong-correlation characteristics linked to Hund's rule coupling of the partially filled t_{2g} orbitals of Ru, which dominate the Fermi surface. The observation of a transition to a superconducting ground state at critical temperature $T_c = 1.5$ K (ref. ⁸), with indirect evidence for proximity to ferromagnetism, led to the suggestion that the pair wave functions of the superconducting state probably exhibit a symmetric spin part, that is, a triplet¹. Crucial support for the existence of a triplet order parameter was provided by NMR spectroscopy, which showed no change in the Knight shift between normal and superconducting states⁵. Later, several experiments produced evidence for time-reversal-symmetry breaking (TRSB)^{9,10}. Together, these reports aligned well to the proposal that Sr_2RuO_4 is a very clean, quasi-two-dimensional solid-state analogue of the topologically nontrivial ³He-A phase¹¹, but in the form of a charged superfluid.

However, several experimental results are difficult to reconcile with the proposed *p*-wave superconducting state¹²⁻¹⁴. For instance, because of TRSB, there is the generic expectation of measurable chiral edge currents (which propagate within a coherence length of the edge, but are screened over a somewhat larger penetration depth scale). However, such currents have not been detected despite several attempts with progressively improved sensitivity¹⁵⁻¹⁷.

In mean-field theory, a chiral p-wave superconductor subjected to in-plane uniaxial strain ε_{aa} exhibits a split transition and an accompanying cusp at about $\varepsilon_{aa} = 0$. However, strained samples of Sr_2RuO_4 exhibit neither; instead, a large increase in T_c (from 1.5 K to 3.5 K) that peaks at $\varepsilon_{aa} = \varepsilon_{v} = -0.5\%$ is observed⁴. This behaviour was interpreted as a consequence of tuning the Fermi energy $E_{\rm F}$ of the quasi-two-dimensional band through a van Hove singularity and a concomitant singularity at ε_v in the density of states (DOS) at E_F (ref. ¹⁸). These observations motivated a study of ¹⁷O NMR in uniaxially pressurized samples; indeed, evidence for the DOS maximum and accompanying enhanced Stoner factor came from normal-state ¹⁷O NMR experiments¹⁹. The results have bearing on the chiral *p*-wave state hypothesis: on the one hand, an odd-parity order parameter vanishes at the location of the van Hove singularity, thereby reducing the impact of the DOS enhancement; on the other hand, the enhanced Stoner factor and ferromagnetic fluctuations could strengthen the pairing instability.

The focus of this paper is the study of $^{17}\rm{O}$ NMR Knight shift on uniaxially pressurized Sr₂RuO₄ by comparing the Knight shifts seen in the normal and superconducting states. The experiments were carried out using a variable-strain device²⁰ (https://razorbillinstruments.com/uniaxial-strain-cell) and cover the full range of $T_{\rm c}=1.5-3.5$ K. $^{17}\rm{O}$ NMR spectroscopy is directly sensitive to the spin polarization $M_{\rm s}$. The expectation for an s-wave (singlet) superconductor is a reduction in the paramagnetic shift, which would vanish in the limit $T/T_{\rm c} \rightarrow 0$ and $B_0/B_{\rm c2} \rightarrow 0$ (where T is the temperature, B_0 is the magnetic field and

Table 1 | Irreducible representations for selected allowed p- and d-wave order parameters compatible with the D_{4h} symmetry of Sr_2RuO_4

Representation	Basis function	Nodes	TRSB	χ_{b0}/χ_{N}
A _{1u}	$\mathbf{d} = \hat{\mathbf{x}}k_x + \hat{\mathbf{y}}k_y$	No	No	1/2
B_{1u}	$\mathbf{d} = \mathbf{\hat{x}} k_x - \mathbf{\hat{y}} k_y$	No	No	1/2
A_{2u}	$\mathbf{d} = \hat{\mathbf{x}} k_y - \hat{\mathbf{y}} k_x$	No	No	1/2
B_{2u}	$\mathbf{d} = \hat{\mathbf{x}} k_y + \hat{\mathbf{y}} k_x$	No	No	1/2
B_{1g}	$\psi_d = k_x^2 - k_y^2$	Vertical	No	0
B_{2g}	$\psi_{d} = k_{x}k_{y}$	Vertical	No	0
E_u	$\mathbf{d} = \hat{\mathbf{z}}(k_x \pm i k_y)$	No	Yes	1
E_u	$\mathbf{d} = k_z (\hat{\mathbf{x}} \pm i \hat{\mathbf{y}})$	Horizontal	Yes	1/2
Eg	$\psi_{\text{chiral}} = k_z (k_x \pm i k_y)$	Horizontal	Yes	0

The two E_u states identified belong to the same irreducible representation and can therefore coexist. Hence, the horizontal nodes of the E_u state with in-plane ${\bf d}$ vector are not protected. Table entries for the ground-state susceptibilities, χ_{LO} , apply to the case ${\bf B} \parallel {\bf b}$ and ignore Fermi liquid corrections and spin-orbit coupling (SOC). For the E_u state, there is no change in the Knight shift for ${\bf B} \parallel {\bf b}$ (refs. $^{2.24,25}$). In the presence of SOC, spin is no longer a good quantum number. Although SOC is relevant to Sr_2RuO_4 (ref. 26), the presence of an inversion centre and time-reversal symmetry in its normal state leads to the conclusion that spin-orbit effects are important only near regions of accidental band degeneracy, which occupy a small fraction of the Brillouin zone, away from areas where the DOS is maximized. Consequently, taking SOC into account will not substantially affect the magnetic responses listed in the fifth column. χ_N is the normal-state spin susceptibility.

¹Department of Physics and Astronomy, University of California Los Angeles, Co. Angeles, CA, USA. ²Wuhan National High Magnetic Field Center and School of Physics, Huazhong University of Science and Technology, Wuhan, China. ³Max Planck Institute for Chemical Physics of Solids, Dresden, Germany. ⁴School of Physics and Astronomy, University of St Andrews, St Andrews, UK. ⁵National Institute for Materials Science, Tsukuba, Japan. ⁶Geballe Laboratory for Advanced Materials, Stanford University, Stanford, CA, USA. ⁷Los Alamos National Laboratory, Los Alamos, New Mexico, USA. ⁸These authors contributed equally: A. Pustogow, Yongkang Luo. *e-mail: pustogow@physics.ucla.edu; mpzslyk@gmail.com; brown@physics.ucla.edu

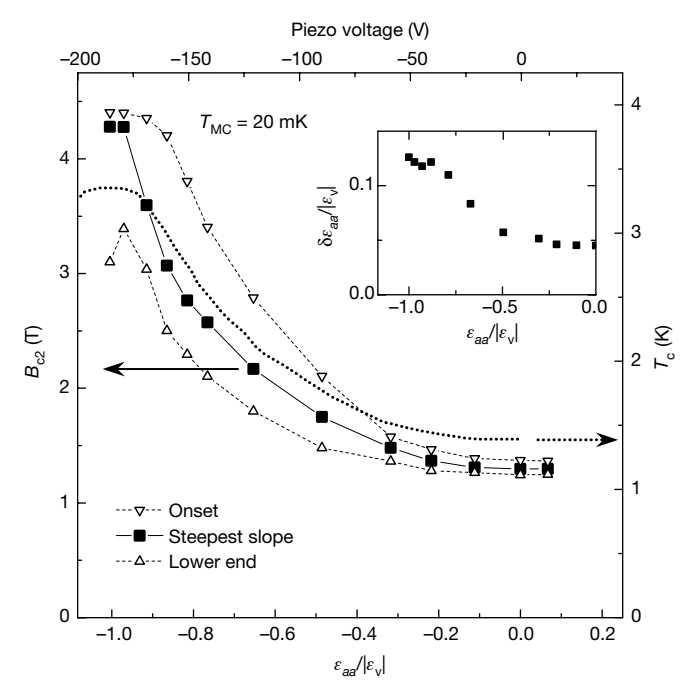


Fig. 1 | Strain dependence of the upper critical field of Sr_2RuO_4 . Upper critical field $B_{c2}(T \to 0, \varepsilon_{aa})$, determined by a.c. susceptibility measurements on a uniaxially strained Sr_2RuO_4 single crystal at a base temperature of T=20 mK. The increase of B_{c2} with compressive strain peaks at ε_{v} , thus closely following the trend of the critical temperature T_c (ref. 4). Inset, strain gradients $\delta\varepsilon_{aa}$ become more pronounced at higher strain, reaching about $0.1\varepsilon_v$ at the van Hove singularity (details in Methods).

 B_{c2} is the upper critical field), whereas for the widely proposed $E_{\rm u}$ state (Table 1), $K_{\rm s}=AM_{\rm s}(B_0)/B_0$ (usually written as the product of a hyperfine coupling A and spin susceptibility χ , $K_{\rm s}=A\chi$, this more general definition allows for a nonlinear response) remains unchanged from the normal-state value. Summarizing the findings, the onset of superconductivity leads to a substantial drop in $M_{\rm s}$ for all strains measured; the zero-strain results are therefore in disagreement with those reported previously⁵. We describe a series of tests that, we believe, account for this discrepancy. Whereas $M_{\rm s}$ remains non-zero for $T\to 0$, quasiparticle creation occurs for several possible reasons in applied fields of $B_0\neq 0$. No evidence for a change in ground-state symmetry is observed as the strain is varied over the interval $\varepsilon_{aa}=[0,\varepsilon_{\rm v}]$.

The crystal structure of $\mathrm{Sr_2RuO_4}$ is identical to that of the undoped parent compound of '214' copper oxides, $\mathrm{La_2CuO_4}$. Likewise, the states at E_F are predominantly of d character; here they derive from hybridization of Ru t_2g and O π orbitals. Extended Data Fig. 1a depicts the orbitals dominating the γ band, associated with the Ru, O(1) and O(1') sites. The O(2) sites are in the apical positions, symmetrically above and below the Ru site. Throughout this report, the magnetic field \mathbf{B}_0 is parallel to \mathbf{b} because out-of-plane field components suppress B_{c2} . On stressing the sample, the relevant response is the resulting asymmetric strain $\varepsilon_{aa} - \varepsilon_{bb}$; only ε_{aa} is noted here.

Because magnetic fields lead to quasiparticle spin polarization, the ideal experiment has an applied field of $B_0 \ll B_{c2}$. Nuclear-spin polarization, on the other hand, favours the largest field possible. For guidance in the choice of experimental parameters, we determined $B_{c2}(\varepsilon_{aa})$ (shown in Fig. 1; see Methods for procedure and uncertainties). B_{c2} is maximized at ε_{v} , coincident with T_c^{\max} , and its value $(4.3 \pm 0.05 \text{ T})$ is within a few per cent of that (4.5 T) reported in ref. ⁴. The reduction could be a result of a small misalignment (of the order of 1°) from the in-plane condition 14,21 . The minimum value is $B_{c2}(\varepsilon_{aa}) = 1.32 \pm 0.05 \text{ T}$, identified by extending the measurements to tensile strains $\varepsilon_{aa} > 0$.

The temperature dependence of the ¹⁷O central transition frequencies for the three sites was measured at $\varepsilon_{aa} = \varepsilon_v$, where B_{c2} is largest, at $B_0 = 1.9980$ T. The resulting spectra, shown in Fig. 2, reveal pronounced changes in the Knight shift, K, upon decreasing the

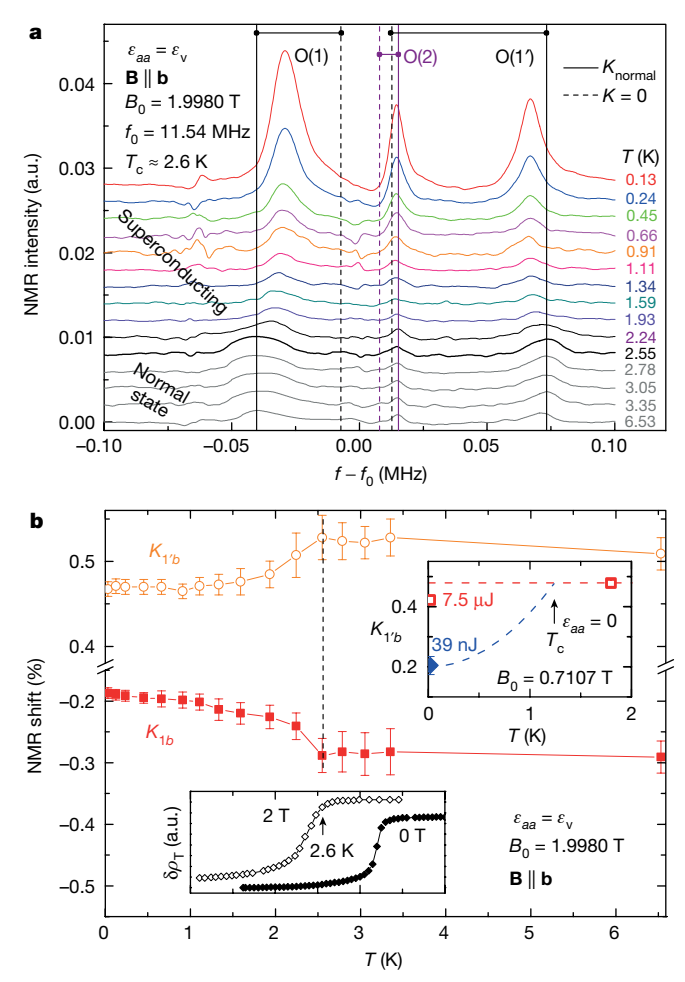


Fig. 2 | Knight shift *K* versus temperature *T*, measured at the van Hove singularity ($\varepsilon_{aa} = \varepsilon_v$). a, NMR spectra measured at an applied field of $B_0 = 1.9980$ T and a carrier frequency of $f_0 = 11.54$ MHz. Shown are three peaks corresponding to the O(1), O(2) and O(1') sites (from left to right). Vertical lines indicate normal-state (solid) and K = 0 (dashed) frequencies. a.u., arbitrary units. b, The associated Knight shifts K_{1b} and $K_{1'b}$ show a pronounced reduction below $T_c(B_0) = 2.6$ K (see lower inset and Methods), indicating a drop in the spin polarization M_s in the superconducting state. $\delta\rho_T$ denotes the change of the reflection coefficient. Upper inset, experiments with varied pulse energy reveal a similar decrease of M_s below T_c for $\varepsilon = 0$ (see Fig. 3 for details). Error bars correspond to 1/4 of the full-width at half-maximum of the peaks in the NMR spectrum.

temperature through $T_c(B_0)$. Because the orbital shifts are relatively small, the frequencies corresponding to K=0 (vertical dashed lines) are attributed to quadrupolar effects¹⁹.

Because the normal-state Knight shifts are $K_{1b} < 0$, $K_{1'b} > 0$, the changes observed for $T < T_c$ in Fig. 2b correspond to a drop of 20-30% in M_s , which is qualitatively different from the zero-strain results⁵. We note that the shifts $K \propto M_s/B_0$ remain non-zero for $T \to 0$, where field-induced quasiparticles are probably relevant at the relatively high fields $(B_0/B_{c2} \approx 0.45)$ used in the measurement. In addition to the contributions from vortex cores, two other sources of local fields should be considered in the context of gap nodes or deep gap minima: the Volovik effect²² and Zeeman coupling, both of which produce quasiparticles and the corresponding magnetic response.

The observed drop in $M_{\rm s}$ upon entering the superconducting state under strained conditions invites a comparison to previous zero-strain experiments, where the lack of reported decrease in $M_{\rm s}$ constituted a cornerstone of the case for a chiral p-wave order parameter. Therefore, we carried out measurements covering the entire interval $\varepsilon_{aa} = [0, \varepsilon_{\rm v}]$, and the results were found to depend on the details of NMR pulsing. With this important observation in mind, a re-examination of the shifts for $\varepsilon_{aa} = 0$ is presented first.

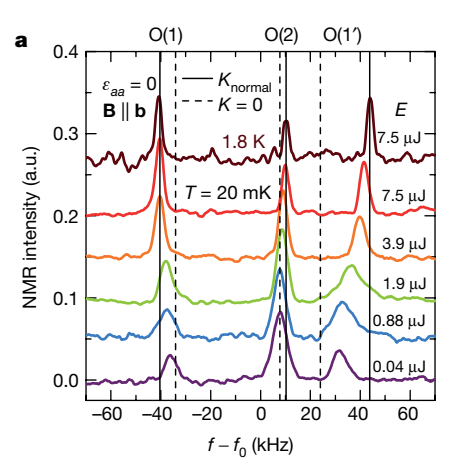
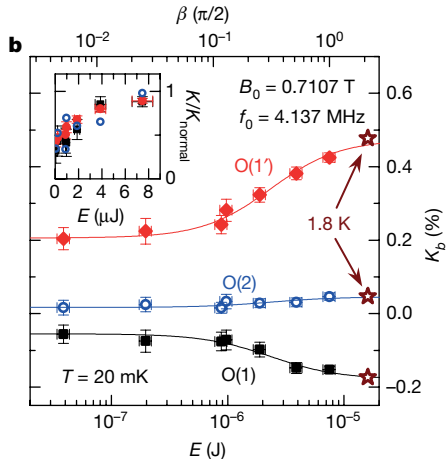


Fig. 3 | Zero-strain $^{17}\mathrm{O}$ NMR spectra of $\mathrm{Sr_2RuO_4}$ for varying pulse energy. a, Free-induction decay measurements with varying pulse lengths $d_1 \leq d_{\pi/2}$ (where $\pi/2$ corresponds to $E=7.5~\mu\mathrm{J}$) were carried out at the nominal base temperature $T_{\mathrm{MC}}=20~\mathrm{mK}$ with $B_0=0.7107~\mathrm{T}$ and $f_0=4.137~\mathrm{MHz}$. The O(1) and O(1') peak shifts indicate smaller M_{S} for smaller E. For each site, the normal-state position is marked by the solid vertical line and the



estimated K=0 position by the dashed line. **b**, Dependence of O(1) and O(1') shifts on the energy (equivalently, the tip angle β). Inset, relative reduction of the Knight shift (with respect to the normal state). We note that the three sites give comparable reductions; uncertainties for the O(2) site are not shown. Error bars as in Fig. 2b.

In Fig. 3 we present spectra collected with no applied stress, following various pulse excitations. The applied field is $B_0 = 0.7107$ T, similar to the 0.65 T field used in ref.⁵, and the temperature of the mixing chamber is $T_{\rm MC} = 20$ mK. We note that from Fig. 1, $B_0/B_{c2}(\varepsilon_{aa} = 0) \approx 0.55$. As above, the three spectral lines shown are the central transitions for O(1), O(2) and O(1'), from low to high frequency. The top trace of Fig. 3a corresponds to the normal state at T = 1.8 K, collected using a standard two-pulse spin echo sequence. The remaining spectra were all recorded at a base temperature of 20 mK and transformed from transients following single-pulse excitations of variable time durations. We note that the single-pulse sequence is much less constraining than the two-pulse spin echo regarding the amount of energy transmitted. These are ordered in Fig. 3a from bottom to top with increasing pulse energy. Figure 3b depicts the shifts versus the pulse energy E; the variations are approximately linear for smaller energies and saturate near the normal-state values for higher energies.

It is tempting to assign the evolution of *K* versus *E* to 'instantaneous' sample heating, such that the spectra are recorded while $T > T_c(B_0)$. Indeed, eddy currents resulting from the high-amplitude radiofrequency pulses provide a mechanism for absorption. Moreover, the heat capacity vanishes continuously in the limit $T \rightarrow 0$. Consequently, a larger temperature increase results from a given amount of energy dissipated at lower temperatures. We note that a check of the nuclear spin–lattice relaxation time T_1 is usually insensitive to such an effect, because the timescales for T_1 and electronic thermal relaxation are so different, $T_1 \gg \tau_{\text{th}}$. Therefore, it is possible that the spectra recorded following high-energy pulses correspond to those of the normal state, whereas the T_1 results correspond to the superconducting state. For insight into the thermal conditions imposed by the radiofrequency pulses, time-synchronous measurements of the power reflected from the tank circuit were carried out. A summary of the conditions is as follows: a radiofrequency pulse (or sequence), such as that used for the NMR excitation, 'pumps' the system. It is followed by a low-power radiofrequency probe, and the reflection is phase-sensitively detected using the NMR receiver. In this way we study the temporal changes in the reflected power, which depends on the sample response to the radiofrequency. We note that this is equivalent to an a.c. susceptibility measurement and relates to radiofrequency shielding. Comparisons to the normal state are possible by measuring also the field dependence, including at $B_0 > B_{c2}$, or by warming to $T > T_c$ ($B_0 = 0$).

Our results for the in-phase and quadrature components of the reflected power are shown in Fig. 4, where the applied pulse energies cover the range used for the NMR measurements. We note that the

overall phase is arbitrary. For sufficiently high-energy pulses, the recovery to a steady state takes place via a two-step process. By comparing to similar measurements carried out in varying fields (see Methods and Extended Data Fig. 4), our interpretation is that the sample under study is initially responding as though it is in the normal state; this lasts for about 100 μs . A second, longer period of relaxation (of the order of 1 ms) occurs within the superconducting state. The longer time is

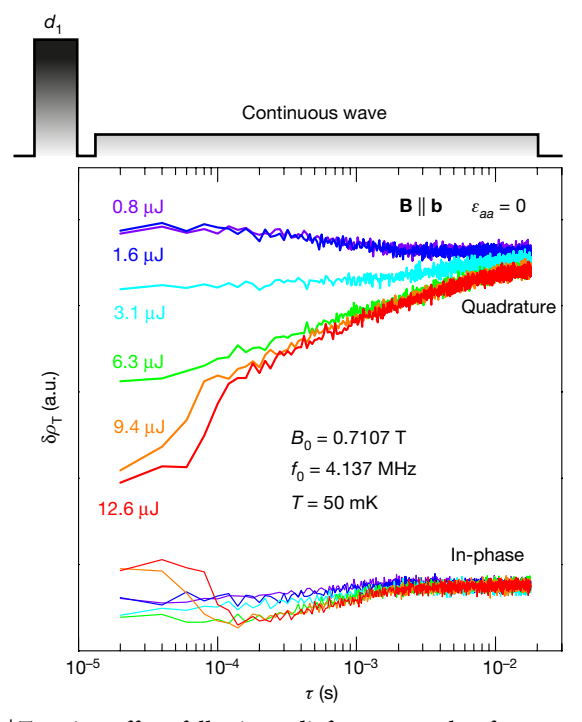


Fig. 4 | Transient effects following radiofrequency pulses for $\varepsilon_{aa}=0$. A short radiofrequency pulse of duration d_1 is applied at time $\tau=0$, followed by a low-power time-resolved continuous wave measurement of the phase-sensitive NMR power reflected from the tank circuit, which is a radiofrequency equivalent to a complex a.c. susceptibility measurement. The data are presented for different pulse energies. Both the in-phase and quadrature parts of $\delta\rho_{\rm T}$ are strongly impacted at short times τ and for larger pulse energies. No similar time dependence is observed when the sample is initially in the normal state.

Table 2 | Quadrupolar corrections to the central transition resonant frequencies, $f={}^{17}\gamma_{\rm n}B_0$, for the three oxygen sites and field strengths applied along the b axis

B (T)	f _{ref} (MHz)	O(1) (kHz)	O(1') _⊥ (kHz)	O(2) _b (kHz)
0.7107	4.0980	1.0	57.5	43.0
1.1573	6.6798	0.8	36.0	26.7
1.9980	11.5323	0.5	20.4	15.6

The listed values apply to the zero-strain case, and we used $^{17}\gamma_n = -5.7719$ MHz T $^{-1}$ (ref. 19).

probably due to a changing vortex structure and motion. No such time dependence is observed if the sample is initially in the normal state.

To summarize the results presented so far, the experiments indicate a reduced spin polarization upon entering the superconducting state at zero strain and at ε_v , with field strengths relative to the upper critical field of $B_0/B_{c2}=0.55$ and 0.45, respectively. An important question is whether there is any indication of a change in order parameter symmetry between these limiting cases. To that end, spectra from normal and superconducting states were recorded for strains covering the interval $\varepsilon_{aa}=[0,\varepsilon_v]$ (see Extended Data Fig. 5 and Methods). The superconducting state data, collected at fields of 0.7107 T and 1.1573 T, vary continuously, with no discernible shift in M_s . Given that one route to a symmetry change is a first-order phase transition, these results, when combined with the smooth variations of B_{c2} (Fig. 1) and the previously measured T_c (ref. 4), suggest that this possibility is unlikely.

The key experimental finding reported here is that at all applied uniaxial pressures, the spin susceptibility deduced from our Knight shift measurements is substantially suppressed at 20 mK compared with the normal-state value. Therefore, for unstrained samples this result is inconsistent with the previously considered $\mathbf{d} = \hat{\mathbf{z}}(k_x \pm ik_y)$ order parameter or indeed any odd-parity state with an out-of-plane \mathbf{d} . Because such order parameters have been widely postulated to be relevant to $\mathrm{Sr}_2\mathrm{RuO}_4$ for over twenty years, this represents a major advance in our understanding of this exemplar of unconventional superconductivity.

Although we can rule out specific odd-parity order parameters of the type described above, we cannot rule out all odd-parity states on the basis of our NMR data alone. In Table 1 we present a summary of the expected changes in Knight shift for symmetry-allowed order parameters in Sr₂RuO₄. A partial drop of the spin susceptibility is predicted in some cases; therefore, the magnitude of the observed drop is important. The uncertainty in estimating the quasiparticle background signal at $B_0/B_{c2} \approx 0.5$ also means that we cannot definitively distinguish odd-parity order parameters with in-plane **d** vectors (such as the A_{1,2u} and B_{1,2u} states in Table 1) from even-parity states at all measured strains. By reducing the measurement field to 0.7107 T, we obtain a 75% drop in the Knight shift at $\varepsilon_{aa} = \varepsilon_{v}$ (see Extended Data Fig. 5). If all of that drop could be attributed to the spin susceptibility, it would indeed rule out all the triplet states listed in Table 1. For the unstrained samples we observe a maximum reduction in Knight shift of approximately 50%—not inconsistent with $A_{1,2u}$ or $B_{1,2u}$ symmetry. We believe that further work on larger samples with higher concentrations of ¹⁷O will allow us to determine whether the true reduction is more than 50% in the unstrained case. We note that reconciling the implications of our results with independent observations of TRSB would require some fine-tuning or unusual physics. For instance, one may consider a situation in which the A_{1u} and B_{1u} states happen to have nearly identical transition temperatures. In that case, one may imagine the formation of distinct domains—some stabilizing the A_{1u} state and others the B_{1u} state, and with non-trivial relative phases between them—resulting in TRSB associated with the domain walls. Because NMR is a local probe, domains of this kind would generally produce distinct line shapes, which we do not observe. In the even-parity sector, the tetragonal crystal field prevents in-plane paired states, such as $d_{x^2-y^2}$ and d_{xy} , from having the same T_c , so the only plausible TRSB order parameter would be of the form $d_{xz} \pm i d_{yz}$ (ψ_{chiral} in Table 1), an exotic state with Cooper

pairing between electrons in adjacent planes. For any bulk TRSB state, however, transition splitting under uniaxial pressure is expected. Because a split transition has not yet been observed, either in our work or elsewhere 23 , extending TRSB-sensitive measurements to strained $\rm Sr_2RuO_4$ is a priority for future work. Overall, these are exciting times for research on $\rm Sr_2RuO_4$, with the promise of a fundamentally different framework with which to understand its superconductivity.

Online content

Any methods, additional references, Nature Research reporting summaries, source data, extended data, supplementary information, acknowledgements, peer review information; details of author contributions and competing interests; and statements of data and code availability are available at https://doi.org/10.1038/s41586-019-1596-2.

Received: 28 March 2019; Accepted: 15 July 2019; Published online 23 September 2019.

- Rice, T. M. & Sigrist, M. Sr₂RuO₄: an electronic analogue of ³He? *J. Phys. Condens. Matter* 7, L643–L648 (1995).
- Mackenzie, A. P. & Maeno, Y. The superconductivity of Sr₂RuO₄ and the physics of spin-triplet pairing. Rev. Mod. Phys. 75, 657–712 (2003).
- Hicks, C. W. et al. Strong increase of T_c of Sr₂RuO₄ under both tensile and compressive strain. Science 344, 283–285 (2014).
- Steppke, A. et al. Strong peak in T_c of Sr₂RuÒ₄ under uniaxial pressure. Science 355, eaaf9398 (2017).
- Ishida, K. et al. Spin-triplet superconductivity in Sr₂RuO₄ identified by ¹⁷O Knight shift. Nature 396, 658–660 (1998).
- Oguchi, T. Electronic band structure of the superconductor Sr₂RuO₄. Phys. Rev. B 51. 1385–1388 (1995).
- Mackenzie, A. P. et al. Quantum oscillations in the layered perovskite superconductor Sr₂RuO₄. Phys. Rev. Lett. 76, 3786–3789 (1996).
- Maeno, Y. et al. Superconductivity in a layered perovskite without copper. Nature 372, 532–534 (1994).
- Luke, G. M. et al. Time-reversal symmetry-breaking superconductivity in Sr₂RuO₄. Nature 394, 558–561 (1998).
- Xia, J., Maeno, Y., Beyersdorf, P. T., Fejer, M. M. & Kapitulnik, A. High resolution polar Kerr effect measurements of Sr₂RuO₄: evidence for broken time-reversal symmetry in the superconducting state. *Phys. Rev. Lett.* 97, 167002 (2006).
- Leggett, A. J. A theoretical description of the new phases of liquid ³He. Rev. Mod. Phys. 47, 331–414 (1975).
- Yonezawa, S., Kajikawa, T. & Maeno, Y. First-order superconducting transition of Sr₂RuO₄. Phys. Rev. Lett. 110, 077003 (2013).
- Hassinger, E. et al. Vertical line nodes in the superconducting gap structure of Sr₂RuO₄. Phys. Rev. X 7, 011032 (2017).
- Kittaka, S. et al. Searching for gap zeros in Sr₂RuO₄ via field-angle-dependent specific-heat measurement. J. Phys. Soc. Jpn 87, 093703 (2018).
- Björnsson, P. G., Maeno, Y., Huber, M. E. & Moler, K. A. Scanning magnetic imaging Sr₂RuO₄. Phys. Rev. B 72, 012504 (2005).
- Hicks, C. W. et al. Limits on superconductivity-related magnetization in Sr₂RuO₄ and PrOs₄Sb₁₂ from scanning SQUID microscopy. *Phys. Rev. B* 81, 214501 (2010).
- Watson, C. A., Gibbs, A. S., Mackenzie, A. P., Hicks, C. W. & Moler, K. A. Micron-scale measurements of low anisotropic strain response of local T_c in Sr₂RuO₄. Phys. Rev. B **98**, 094521 (2018).
- Sunko, V. et al. Direct observation of a uniaxial stress-driven Lifshitz transition in Sr₂RuO₄. npj Quantum Mater. 4, 46 (2019).
- Luo, Y. et al. Normal state ¹⁷O NMR studies of Sr₂RuO₄ under uniaxial stress. Phys. Rev. X 9, 021044 (2019).
- Hicks, C. W., Barber, M. E., Edkins, S. D., Brodsky, D. O. & Mackenzie, A. P. Piezoelectric-based apparatus for strain tuning. *Rev. Sci. Instrum.* 85, 065003 (2014).
- Kittaka, S. et al. Angular dependence of the upper critical field of Sr₂RuO₄. Phys. Rev. B 80, 174514 (2009).
- Volovik, G. E. Superconductivity with lines of GAP nodes: density of states in the vortex. JETP Lett. 58, 469–473 (1993).
- 23. Li, Y. S. et al. High precision heat capacity measurements on Sr_2RuO_4 under uniaxial pressure. Preprint at http://arxiv.org/abs/1906.07597 (2019).
- 24. Vollhardt, D. & Woelfle, P. The Superfluid Phases of Helium 3 (CRC Press, 1990).
- Matano, K., Kriener, M., Segawa, K., Ando, Y. & Zheng, Q. G. Spin-rotation symmetry breaking in the superconducting state of Cu_xBi₂Se₃. Nat. Phys. 12, 852–854 (2016).
- Veenstra, C. N. et al. Spin-orbital entanglement and the breakdown of singlets and triplets in Sr₂RuO₄ revealed by spin- and angle-resolved photoemission spectroscopy. *Phys. Rev. Lett.* **112**, 127002 (2014).

Publisher's note Springer Nature remains neutral with regard to jurisdictional claims in published maps and institutional affiliations.

© The Author(s), under exclusive licence to Springer Nature Limited 2019

METHODS

Experimental. The geometry of the experiment is shown in Extended Data Fig. 1. The crystal structure consists of layers of corner-sharing O octahedra with Ru ions at the centre of each octahedron. In Extended Data Fig. 1a, we illustrate the planar coordination (at the Y point of the Brillouin zone) of hybridizing Ru and O orbitals that dominate the quasi-two-dimensional γ -band character. An in-plane magnetic field ${\bf B}_0 \parallel {\bf b}$ yields inequivalent O(1) and O(1') sites with distinct Knight shifts. Uniaxial deformation along the a axis pushes the γ states at $E_{\rm F}$ towards the Brillouin zone boundary (Extended Data Fig. 1b), giving rise to a van Hove singularity in the DOS^{4,19}.

The high-quality single-crystalline $\rm Sr_2RuO_4$ used for these measurements was grown by the floating-zone method as described elsewhere⁸. Smaller pieces were cut and polished along the crystallographic axes with typical dimensions of $3\times0.3\times0.15~\rm mm^3$, with the longest dimension aligned with the a axis. Spin-labelling of the $^{17}\rm O$ isotope (nuclear spin $^{17}I=5/2$; gyromagnetic ratio, $^{17}\gamma_n=-5.7719~\rm MHz~T^{-1})^{27}$ was achieved by annealing in 50% $^{17}\rm O$ -enriched oxygen atmosphere at 1,050 °C for two weeks⁵. The sample quality after annealing was confirmed by specific-heat measurements, which showed $T_c\approx1.5~\rm K$ —essentially the same as before annealing 19 .

A piezoelectric-type strain cell (Razorbill) was employed to generate the uniaxial stress and corresponding strain distortions along the a axis. The sample was mounted between clamping plates using black Stycast 2850 (Loctite) with an effective compressive length of about 0.9 mm. The strain values ε_{aa} estimated using a pre-calibrated capacitive dilatometer showed considerable systematic overestimation. Previous estimates gave $\varepsilon_{\rm v}\approx-0.6\%$. For the NMR measurements, a small coil of ~23 turns was made around the sample with 25-µm Cu wire. In Extended Data Fig. 1c we show the sample mounted in the strain cell, where $\varepsilon_{aa} \parallel {\bf a}$ and ${\bf B}_0 \parallel {\bf b}$. The NMR coil was wrapped around the free part of the crystal, thus covering only the non-glued area that was subject to uniaxial stress. More information on strain-dependent NMR experiments on ${\rm Sr_2RuO_4}$ can be found in ref. 19 .

The NMR measurements were performed using a standard spin echo sequence with an external magnetic field parallel to the b axis. Two samples were measured, denoted as S1 and S2. S1 was measured at fixed strain $\varepsilon_{aa} = \varepsilon_v \ (T_c = T_c^{max} = 3.5 \ K)$ and carrier frequency $f_0 = 11.54$ MHz ($B_0 = 1.9980$ T) at temperatures spanning both sides of T_c . Two sets of measurements were carried out on S2. First, a fixed carrier frequency of $f_0 = 6.7$ MHz ($B_0 = 1.1573$ T) was used for measurements at temperatures of 20 mK (superconducting state) and 4.3 K (normal state) as a function of strain up to -0.58%. The second set of strain-dependent measurements in the superconducting state (T = 20 mK) was performed at $f_0 = 4.137 \text{ MHz}$ $(B_0 = 0.7107 \text{ T})$, followed by a detailed study at zero strain. All measurements on S2 were conducted using a dilution refrigerator (Oxford Kelvinox) with the entire strain jig, including the Sr₂RuO₄ crystal, immersed inside the mixing chamber. The magnetic field value B_0 was referenced to the 3 He NMR condition at f_0 . The temperature of the mixing chamber $T_{\rm MC}$ = 20 mK was confirmed by a measurement of the relaxation time T_1 of 63 Cu (in the coil), and using the accepted value $T_1T = 1.27 \text{ s K}$

NMR shift correction for quadrupolar splitting. The NMR Knight shift, K, is generically defined as the percentage of the shift of resonance frequency with respect to a reference frequency $f_{\rm ref}={}^{17}\gamma_{\rm n}B_0$, namely, $f={}^{17}\gamma_{\rm n}B_0(1+K)$. However, an additional field-dependent correction is necessary for nuclei with I>1/2, owing to quadrupolar coupling to the electric-field gradient. On a relative scale, the angle-dependent correction to the central transition is more important in weaker fields. It is numerically evaluated by diagonalizing the nuclear-spin Hamiltonian

$$H_{\text{tot}} = H_{\text{Z}} + H_{\text{O}} \tag{1}$$

where

$$H_{\mathbf{Z}} = h^{17} \gamma_{\mathbf{p}} (1 + K) \mathbf{B}_{0} \cdot \hat{\mathbf{I}}$$
 (2)

characterizes the Zeeman effect, and

$$H_{Q} = \frac{eQV_{zz}}{4I(2I-1)} \left[3\hat{I}_{z}^{2} - \hat{\mathbf{I}}^{2} + \eta (\hat{I}_{x}^{2} - \hat{I}_{y}^{2}) \right]$$
 (3)

is the quadrupolar term. Here, h is Planck's constant, $\hat{\bf l}=(\hat{l}_x,\hat{l}_y,\hat{l}_z)$ is the nuclear spin operator, Q is the nuclear quadrupole moment, e is the electron charge and $\eta=(V_{xx}-V_{yy})/V_{zz}$ is the asymmetry parameter, with V_{xx} , V_{yy} and V_{zz} being the components of the electric-field gradient tensor. For the magnetic fields used in this work, the calculated corrections for different $^{17}{\rm O}$ sites are listed in Table 2.

Upper critical field measurements and estimation of strain gradients. As summarized in Fig. 1, the upper critical field $B_{\rm c2}$ is determined at a base temperature of $T_{\rm MC}=20$ mK by measuring the field dependence of the power reflected from the NMR tank circuit. Specifically, the frequency is set close to the optimal tuning and matching condition of the NMR circuit. Variations in the reflection

coefficient $\delta \rho_T$ relate to changes in the complex load impedance. Consequently, the measurement is equivalent to an a.c. susceptibility experiment and is sensitive to screening current changes that occur, for example, when the system is driven from the superconducting to the normal state by the magnetic field. B_{c2} is taken as the steepest slope at the transition midpoint, that is, the maximum of $d(\delta \rho_T)$ dB_0 (Extended Data Fig. 2a, b), for the respective strain potential bias, U_{Piezo} . The uncertainty in determining B_{c2} is taken as the half width of $d(\delta \rho_T)/dB_0$, for example, $B_{c2}=4.3\pm0.05$ T at $\varepsilon_{aa}=\varepsilon_{v}$. The 'onset' and 'lower end' values are defined as the kinks in the derivative $d(\delta \rho_T)/dB_0$ above and below B_{c2} , respectively. The superconducting transition exhibits considerable broadening with increasing compressive strain ε_{aa} . To model the apparently smeared transition, we assume a Gaussian distribution of strains and use the resulting distribution in B_{c2} to generate the solid magenta curves in Extended Data Fig. 2. The curves shown correspond to strain variations of 10% of the normalized value, $\varepsilon_{aa}/\varepsilon_{v}$ (see inset of Fig. 1). This approach provides a self-consistent method for estimating the relative importance of strain distributions and suitably describes our observations.

Assessing the zero-strain position. The zero-strain condition attributed to the spectra shown in Fig. 3 is determined by taking the minimum in $B_{\rm c2}$ as a proxy. We note that because there is differential thermal contraction between the strain device and the sample, the strain-free condition needs to be assessed in situ. This determination is carried out in two steps. First, for a range of discrete positive and negative values of piezo bias $U_{\rm Piezo}$ around 0 V, $B_{\rm c2}(U_{\rm Piezo})$ is determined by using field sweeps and recording the reflected power, as for the measurements in Fig. 1 and Extended Data Fig. 2. Example sweeps are shown in Extended Data Fig. 3a, b, from which the minimum is found to be near $U_{\rm Piezo} = 0$ V. A more accurate determination is made by first setting the initial field to $B_{\rm c2}(U_{\rm Piezo} = 0$ V), that is, to the transition midpoint, as shown in the inset of Extended Data Fig. 3c. Then, changes in reflected power are recorded by sweeping $U_{\rm Piezo}$ about zero. Here again we find the zero-strain condition to be indistinguishable from $U_{\rm Piezo} = 0$ V. Thus, our experiments at low pulse energy indeed probe the superconducting properties of $S_{\rm T2}RuO_a$ at zero strain.

Time-synchronous reflected-power response. Our interpretation of the time-synchronous reflected-power measurements was aided by comparative measurements carried out in variable-field conditions, with the goal to contrast normal- and superconducting-state responses. The results are shown in Extended Data Fig. 4, where the applied pulse energies cover the range used for the NMR measurements. Extended Data Fig. 4b shows a measurement of the power reflected from the NMR tank circuit as the magnetic field is varied to a strength exceeding B_{c2} . The jump at 1.3 T corresponds to the transition to the normal state. The evolution at lower fields is presumably associated with the response of a changing vortex structure, including density and characteristic length scales. The vertical dashed line indicates the field used for the measurement of the spectra shown in Fig. 3, $B_0 = 0.7107$ T. Both the in-phase and quadrature components of $\delta\rho_T$ show a pronounced time dependence for large pulse energies. Our interpretation is that the sample under study is initially responding as though it is in the normal state. The relaxation back to the static superconducting state that is appropriate for the applied field occurs via a two-step relaxation process. First, it is in the normal state for $\tau \le 100 \, \mu s$, followed by a slower relaxation of a few milliseconds while in the superconducting state. The horizontal dotted lines in Extended Data Fig. 4 indicate the values of $\delta \rho_T(B_0)$ right above and below the superconducting transition, as well as the static state at 0.7107 T. The longer relaxation time is probably due to changing vortex structure and motion. No such time dependence is observed if the sample is initially in the normal state.

Strain-dependent NMR shifts. The results of the strain-dependent studies of the NMR Knight shifts are shown in Extended Data Fig. 5, with data from the superconducting state depicted by open symbols (equilibrium temperature of 20 mK) and those from the normal state indicated by solid symbols (equilibrium temperature of 4.3 K)¹⁹. In addition to the results shown in Fig. 2 (green symbols; T = 20 mK, $B_0 = 1.9980$ T), two different fields are shown for each temperature. The suppression of the Knight shift in the superconducting state reaches about 80% for strain near ε_v in the case of $B_0 = 0.7107$ T (blue). The effect of superconductivity weakens upon lowering the strain, as T_c and B_{c2} both decrease. Because the spectra are generated by the standard echo sequence for these data, the pulse energies are large—about $E \approx 10 \,\mu\text{J}$, which is comparable to the top trace in Fig. 3. Thus, the results at low and zero strain correspond to the normal-state shifts; this is very obvious in the results at 20 mK and 1.1573 T (orange), which deviate from the 4.3 K data only for $\varepsilon_{aa} > \varepsilon_v/2$. Although the reduction of K is generally more pronounced for 0.7107 T, these data also approach the normal-state values when $\varepsilon_{aa} \rightarrow 0$. Evidently, the impact of the pulse energy decreases when the sample is strained because T_c increases and the heating effect is not sufficiently strong to drive the crystal to the normal state. The results appear to vary continuously with applied field and strain, hence they provide no indication of a first-order phase transition between different superconducting order parameter symmetries.



Data availability

The data that support the findings of this study can be accessed at http://www.pa.ucla.edu/content/sr2ruo4-knightshift. Additional information is available from the corresponding authors upon reasonable request.

 Hoult, D. I. in eMagRes (eds Harris, R. K. & Wasylishen, R. L.) (John Wiley & Sons, 2007).

Acknowledgements We thank M. Ikeda and S. Kivelson for conversations. We particularly appreciate discussions with K. Ishida and Y. Maeno about the implications of our findings, and K. Ishida for reproducing our results. A.P. acknowledges support by the Alexander von Humboldt Foundation through a Feodor Lynen Fellowship. Y.L. acknowledges support by the 1000 Youth Talents Plan of China. N.K. acknowledges support from JSPS KAKENHI (number JP18K04715) and JST-Mirai Program (number JPMJMI18A3) in Japan. S.R. is supported in part by the US Department of Energy, Office of Basic Energy Sciences, contract DEAC02-76SF00515. This work was supported in part by the National Science Foundation (DMR-1709304) and by the Laboratory Directed

Research and Development (LDRD) programme of Los Alamos National Laboratory under project number 20170204ER.

Author contributions Y.L., A.P., A.P.M. and S.E.B. conceived and designed the experiments. D.A.S., N.K., F.J., C.W.H. and A.P.M. prepared the crystal. E.D.B. characterized the sample and performed the spin labelling. A.P. and Y.L. performed the NMR measurements, supported by Y.-S.S. and A.C.; A.P., Y.L., C.W.H., A.P.M., S.R. and S.E.B. discussed the data, interpreted the results and wrote the paper with input from all authors. The time-synchronous reflection experiments were performed by S.E.B., A.P. and A.C.

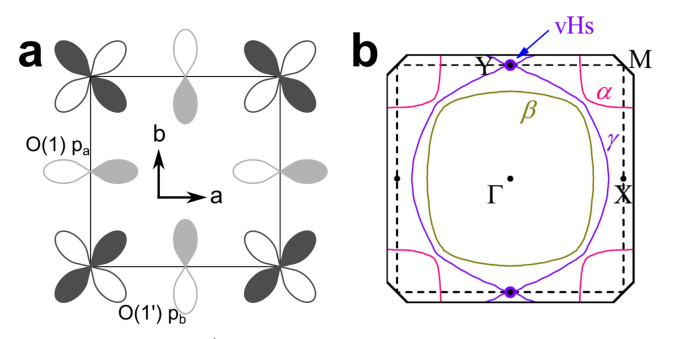
Competing interests The authors declare no competing interests.

Additional information

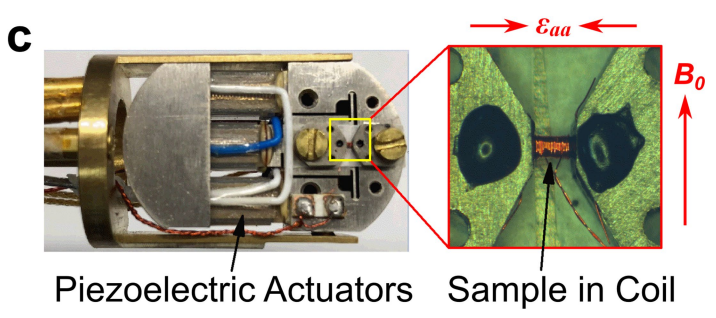
Correspondence and requests for materials should be addressed to A.P., Y.L. or S.F.R.

Peer review information *Nature* thanks Catherine Kallin, Guo-qing Zheng and the other, anonymous, reviewer(s) for their contribution to the peer review of this work. **Reprints and permissions information** is available at http://www.nature.com/reprints

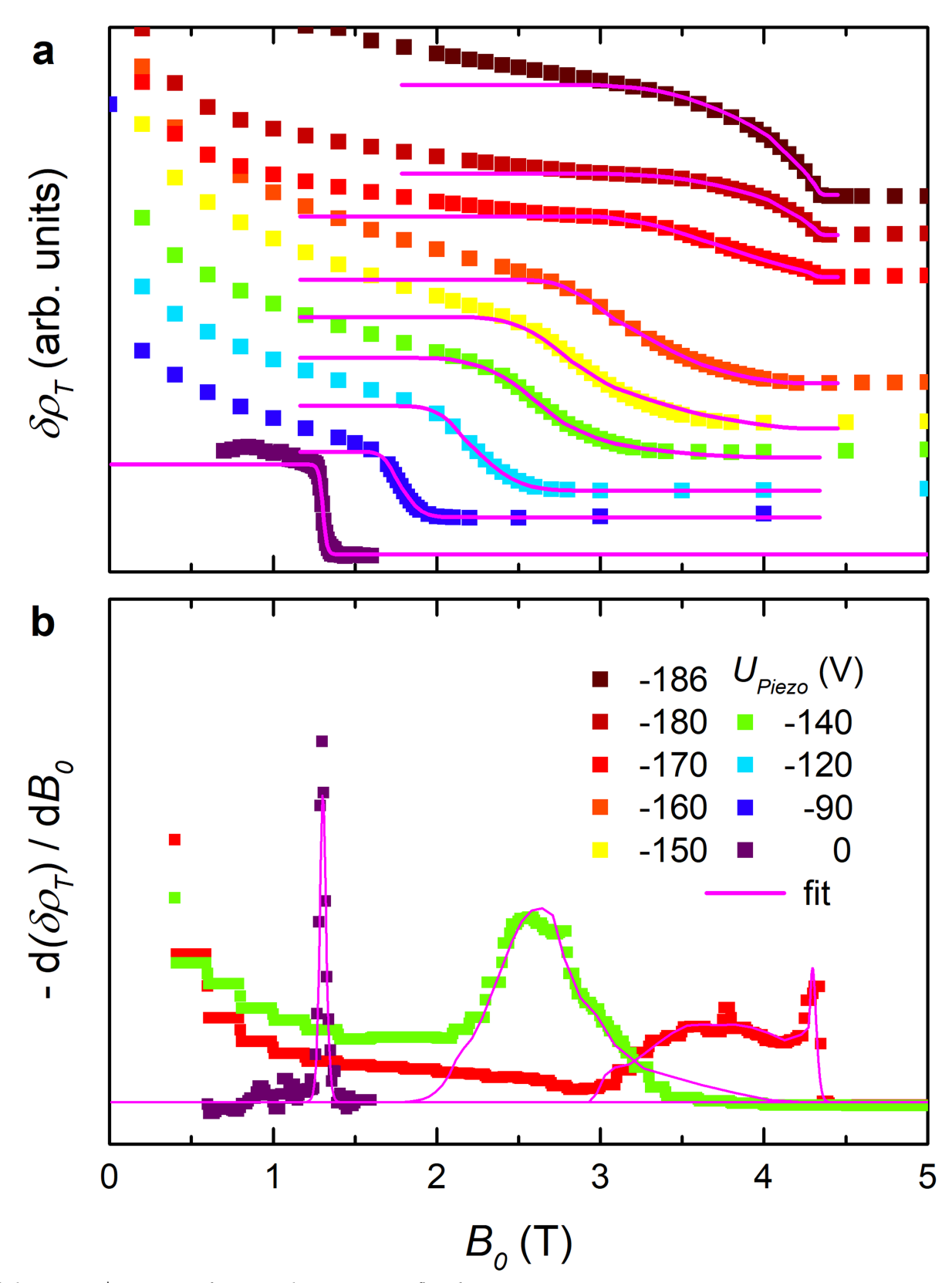




Extended Data Fig. 1 | RuO₂ plane, with $d_{xy}-p$ hybridizing orbitals and experimental setup. a, Ru d_{xy} and hybridizing O p orbitals at the Y point, which dominate the formation of the γ band. NMR shifts are measured at the O(1) and O(1') sites. b, Compressive a-axis stress shifts the γ -band Fermi surface to the zone boundary at Y. vHs, van Hove singularity. c,

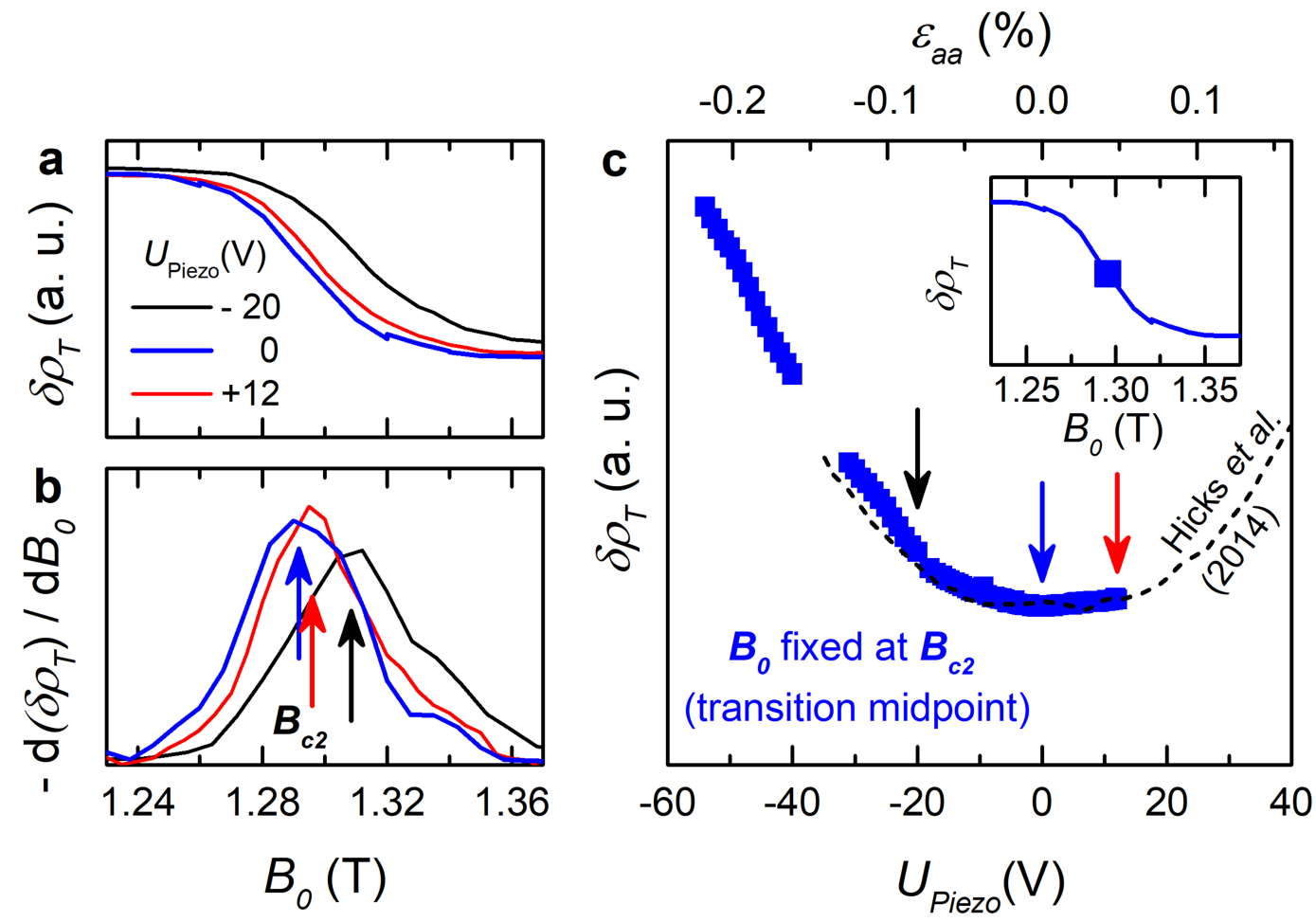


Strain device. The enlarged view highlights the $\mathrm{Sr}_2\mathrm{RuO}_4$ single crystal mounted between the piezoelectric actuators, with B_0 parallel to the b axis and the compressive stress along the a axis, ε_{aa} . The NMR coil covers the free part of ~1 mm length.



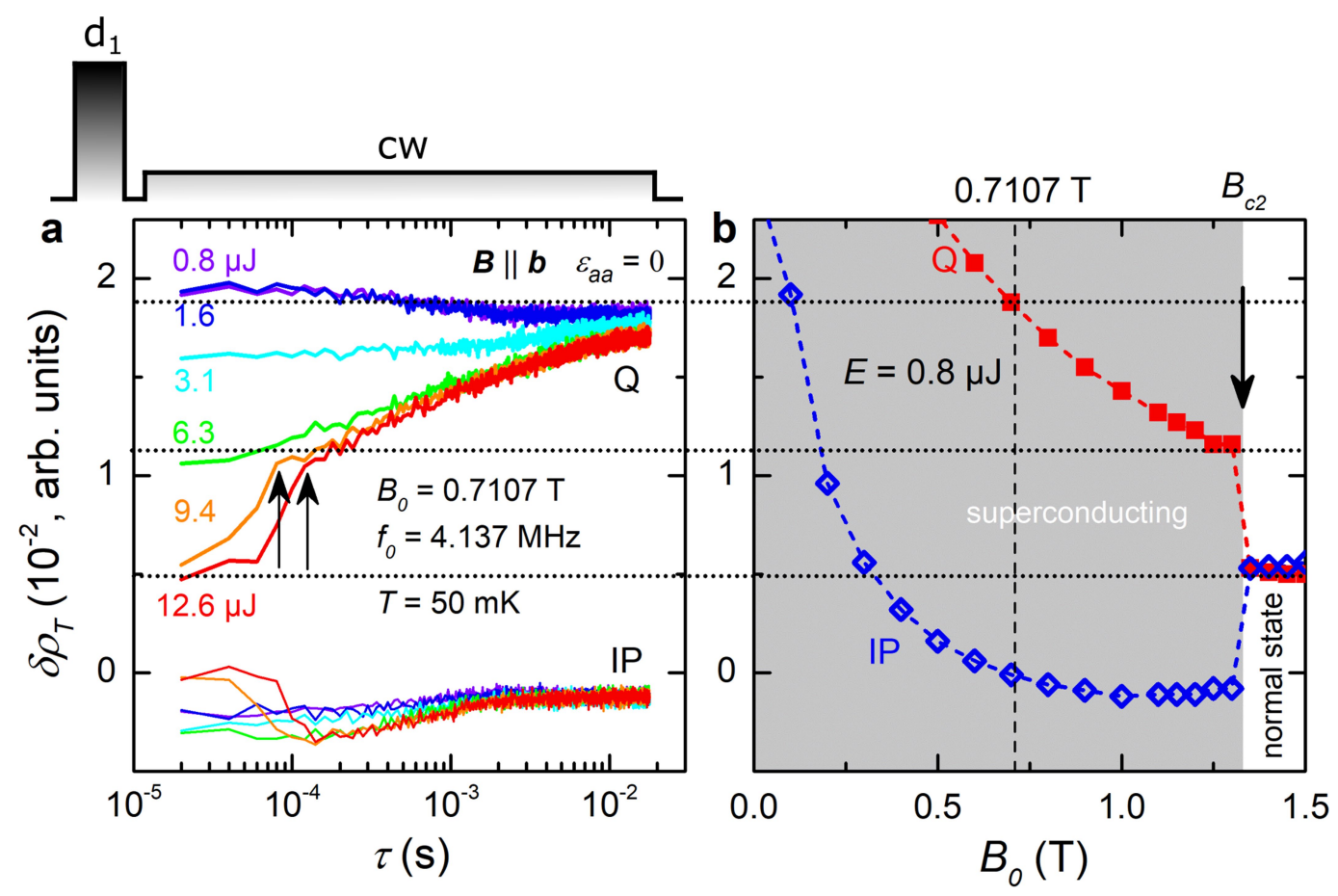
Extended Data Fig. 2 | **Estimation of strain gradients. a**, Power reflected from the tank circuit during magnetic-field sweeps. The steepest slope of $\delta \rho_{\rm T}(B_0)$ corresponds to the $B_{\rm c2}$ values shown in Fig. 1. The broadening of the superconducting transition was modelled by a Gaussian strain

distribution of half-width $\delta \varepsilon / \varepsilon_{aa} \approx 10\%$ (pink lines). **b**, The fitting curves also match with the corresponding derivative $d(\delta \rho_T)/dB_0$. For clarity, only a subset of the measured fields is shown.



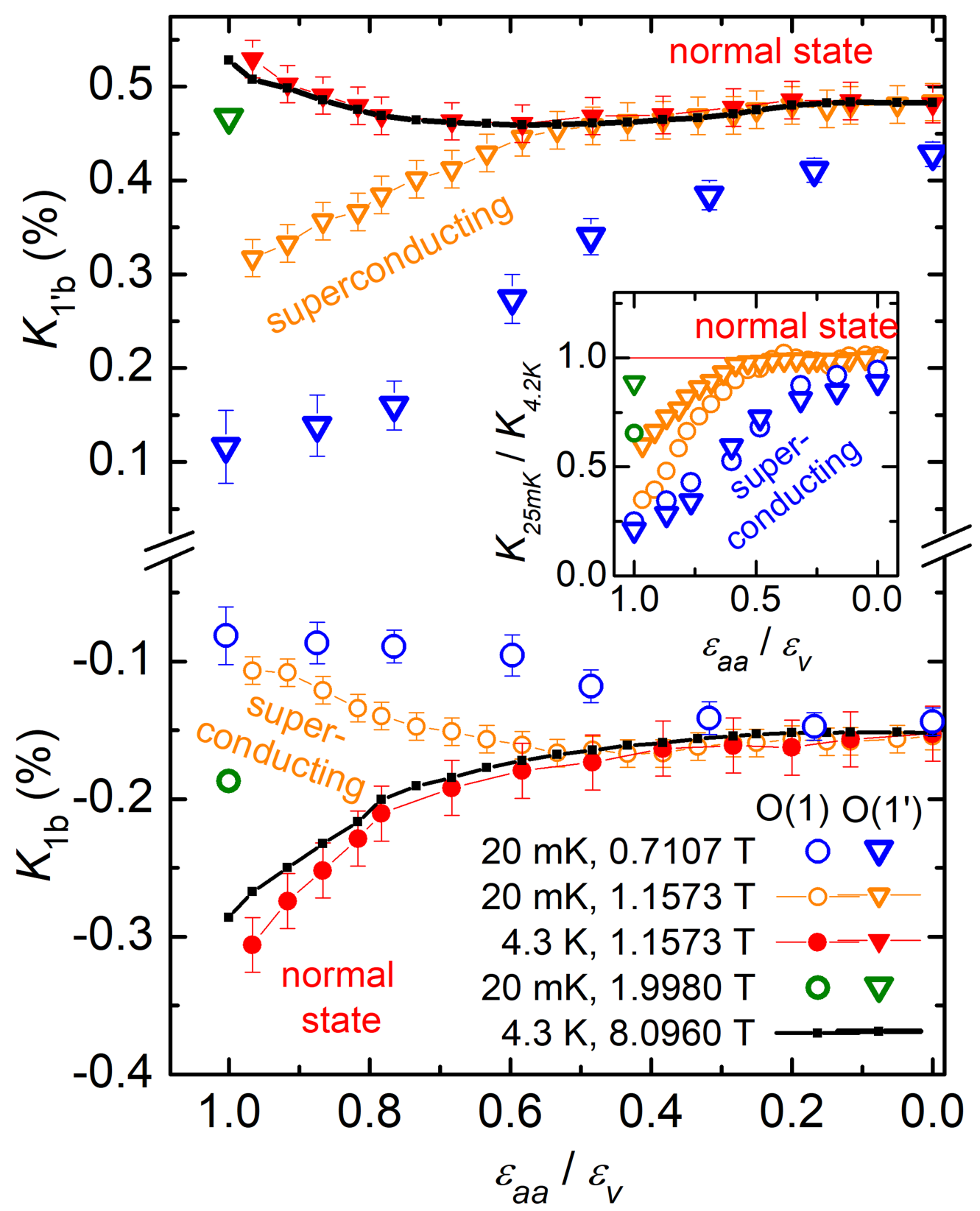
Extended Data Fig. 3 | Tuning of the crystal to zero strain. a, Measurements of the reflected power $\delta\rho_{\rm T}$ at low strain indicate that $B_{\rm c2}$ has a minimum near $U_{\rm Piezo}=0$ V. b, The derivative ${\rm d}(\delta\rho_{\rm T})/{\rm d}B_0$ illustrates that the $B_{\rm c2}$ value associated with the largest rate of change at the transition midpoint first decreases when reducing the compression ($U_{\rm Piezo}$ changing from -20 V to 0 V), followed by a slight increase upon tensile strain ($U_{\rm Piezo}$ changing from 0 V to +12 V). c, The coil impedance was measured

at the transition midpoint (B_0 fixed at B_{c2} , as indicated in the inset), providing a sensitive measure of modifications upon changing the strain. B_{c2} was determined by a field sweep at intervals of 20 V or less, and then B_0 was set to the new transition midpoint. The results (solid blue squares) were corrected for the different B_0 values, yielding one half of a parabola centred around [-10 V, 10 V], very similar to the strain dependence of T_c reported in ref. 3 (dashed black line).



Extended Data Fig. 4 | Transient effects associated with normal-state response. a, The transient components of the reflected power are plotted as a function of pulse energy E and time τ after the pulse (see Fig. 4). CW, continuous wave; IP, in-phase; Q, quadrature. b, The magnetic-field dependence of the reflected power was recorded at $E=0.8 \mu J$. The changes

in $\delta \rho_{\rm T}(B_0)$ for increasing B_0 from the measurement field (0.7107 T) to $B_0 > B_{\rm c2}$ match well with the time-dependent recovery in ${\bf a}$, as indicated by the horizontal dotted lines. Both channels (IP and Q) indicate a variation in $\delta \rho_{\rm T}$ that results from a transition between normal and superconducting states around $\tau \approx 100~\mu \rm s$.



Extended Data Fig. 5 | Strain dependence of ¹⁷O Knight shifts in the superconducting and normal states. Comparison of shifts in the normal and superconducting states for strains covering the range $\varepsilon_{aa} = [0, \varepsilon_v]$. The top and bottom parts of the figure show the O(1') and O(1) sites, respectively. The normal-state results (indicated by black and red solid symbols) were recorded at 4.3 K and two different field strengths¹⁹. Open

symbols correspond to an equilibrium temperature of 20 mK, which is within the superconducting state for sufficiently high $T_{\rm c}$, realized by large strain and small magnetic field. Blue and orange symbols correspond to field strengths of 0.7107 T and 1.1573 T, respectively. The results for $B_0=1.9980$ T are shown in green ($\varepsilon_{aa}=\varepsilon_{\rm v}$; see Fig. 2).